

pubs.acs.org/cm Article

Effectiveness of Different Ligands on Silane Precursors for Ligand Exchange to Etch Metal Fluorides

Ann Lii-Rosales, Virginia L. Johnson, Andrew S. Cavanagh, Andreas Fischer, Thorsten Lill, Sandeep Sharma, and Steven M. George*



Cite This: Chem. Mater. 2022, 34, 8641-8653



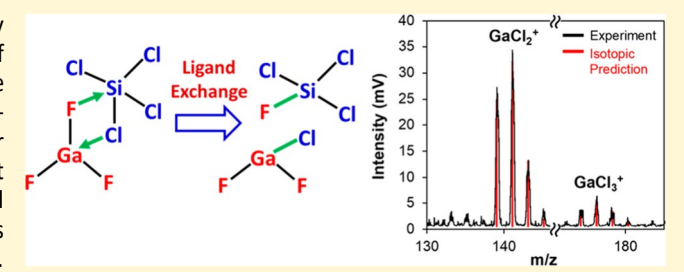
ACCESS

III Metrics & More

Article Recommendations

Supporting Information

ABSTRACT: Metal fluorides can be spontaneously etched by ligand-exchange reactions. During these reactions, the exchange of ligands between the incoming precursor and the metal fluoride leads to the volatilization of the metal fluoride. These ligand-exchange reactions are important in many thermal atomic layer etching (ALE) processes. To test the effectiveness of different ligands for ligand exchange, the spontaneous etching of metal fluorides by silane precursors containing different ligands was investigated using *in situ* quadrupole mass spectrometry (QMS). The homoleptic and heteroleptic silane precursors were SiCl₄



SiCl₂(CH $_3$ 2 SiCl(CH $_3$ $_4$, and Si(CH $_3$ $_3$. These silane precursors provide CI, CH , of H ligands for the ligand-exchange reaction. The metal fluorides were GaF , InF₃ , ZnF₃ , ZrF₂ , HfF₄ , and₄SnF . The₄QMS results showed that F/CI ligand exchange was observed for all the metal fluorides with chlorine-containing silane precursors. In addition, all the volatile metal etch products were metal chlorides, namely, GaCl , InCl , ZrCl , HfCl , and SnCl . No metal methyl complexes were detected as volatile metal etch products indicating no F/CH exchange, For SiCl(CH) H as the silane precursor, the observation of SiF (CH) indicated that F/H exchange is also possible in addition to F/Cl exchange. For the various metal fluorides, the dominance of the F/Cl exchange led to nearly equivalent onset temperatures for ligand exchange and for etching to yield metal chlorides. Thermochemical calculations of the ligand-exchange reactions also predicted the formation of metal chlorides. All F/Cl exchanges were the most thermodynamically favorable as demonstrated by their negative changes in Gibbs free energy (ΔG). These experimental and theoretical results provide guidelines for designing precursors for thermal ALE processes.

1. INTRODUCTION

Thermal atomic layer etching (ALE) is a gas phase etching technique that utilizes sequential and self-limiting surface reactions. The reactions consist of a surface modification step followed by volatile release of the modified surface. For the thermal ALE of metal oxides such as Al_2O_3 , HfO_2 , and ZrO_2 , the modification step typically involves fluorination using HF. The volatile release step can then employ a ligand-exchange reaction that can be characterized as a transmetalation reaction. During the ligand-exchange reaction, the ligands on the precursor are exchanged with the F ligands in the metal fluoride.

Various precursors have been demonstrated for ligand exchange in thermal ALE such as AI(CH₃)₃, AICI(CH₃)₂, SiCl₄, TiCl₄, BCl₃, Ga(N(CH₃)₂)₃, and Sn(acac)₂. ^{1-11,13,14} Most of these precursors contain ligands such as CI and CH₃. These are effective ligands for volatile release if the reaction can produce stable and volatile metal chlorides or metal methyl complexes. Out of the various precursors demonstrated for ligand exchange in thermal ALE, only SiCl₄ is a silane precursor. ⁸ Silanes are an important class of precursors for ligand exchange with metal fluorides because of strong Si-F

covalent bonding.¹⁵ The Si–F bond formation can be a substantial thermochemical driving force for ligand exchange. In addition, Si can form complexes with a wide variety of ligands. Consequently, silane precursors containing different ligands are an excellent testbed for exploring the effectiveness of various ligands for ligand exchange in thermal ALE.

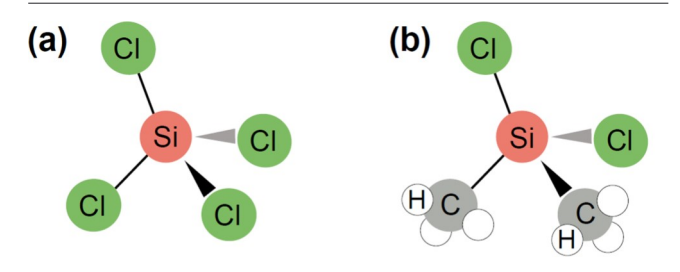
This work explores the spontaneous etching of metal fluorides with silane precursors. The spontaneous etching models the volatile release of the surface fluoride in thermal ALE. The spontaneous etching reactions were studied using a reactor equipped with sample heating and *in situ* quadrupole mass spectrometry (QMS). Six different metal fluorides were studied including GaF₃, InF₃, ZnF₂, ZrF₄, HfF₄, and SnF₄. These metal fluorides represent the corresponding metal oxides after fluorination in the surface modification step during

Received: May 28, 2022
Revised: September 2, 2022
Published: September 19, 2022





thermal ALE. Four different homoleptic and heteroleptic silane precursors were explored for ligand exchange including SiCl₄, SiCl₂(CH₃)₂, SiCl(CH₃)₂H, and Si(CH₃)₄. These silane precursors are shown in Figure 1. Only SiCl₄, together with HF for fluorination, has been previously employed for ligand exchange during the thermal ALE of HfO₂ and ZrO₂.⁸



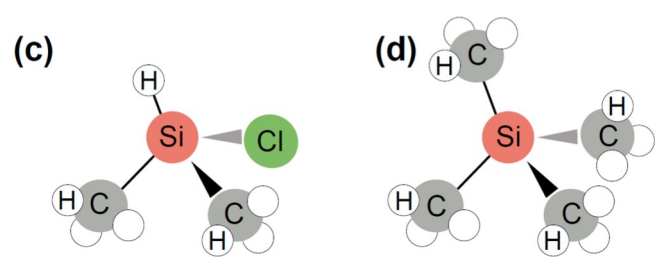


Figure 1. Pictures of the silane precursors: (a) $SiCl_4$ (silicon tetrachloride), (b) $SiCl_2(CH_3)_2$ (dichlorodimethyl-silane), (c) $SiCl_2(CH_3)_2H$ (chlorodimethyl-silane), and (d) $Si(CH_3)_4$ (tetramethyl-silane).

The various silane precursors allow the F/Cl, F/CH₂, and F/ H exchange reactions to be studied by monitoring the ligandexchange and metal etch products using in situ QMS investigations. 16 The relative importance of F/Cl, F/CH₂, and F/H exchange reactions can be determined by measuring the intensity of the ligand-exchange and metal etch products and their temperature dependence. In addition, the ligandexchange reactions must be thermodynamically favorable to generate stable and volatile products. Thermochemical calculations were performed to determine the change in Gibbs free energy (ΔG) for each combination of the different silane precursors with the various metal fluorides. These experimental and theoretical studies help to clarify the importance of the specific ligand during ligand-exchange reactions. This understanding is also useful for the design of effective reactants for thermal ALE.

2. EXPERIMENTAL SECTION

2.1. Quadrupole Mass Spectrometry (QMS) Reactor. Detection of volatile species during the ligand-exchange reactions was accomplished using a reactor equipped with *in situ* QMS (Extrel, MAX-QMS Flange Mounted System). The QMS reactor was also equipped with a sample housing that could be heated to obtain a temperature ramp. Typical temperature ramps were 3 °C/min and ranged from room temperature at 20 °C to a limiting temperature of 530 °C. All volatile species were entrained in a N₂ molecular beam and delivered line-of-sight to the QMS ionizer entrance. This configuration allowed for direct and accurate analysis of the volatile species.

The metal fluoride powder was placed in the sample housing. N_2 was flowed through the sample housing together with the silane precursors. ¹⁶ The typical operating pressure inside the sample housing

was 2–3 Torr under the N_2 viscous flow. The pressure in the differentially pumped area outside the sample housing was in the low 10^{-5} Torr range. The differentially pumped QMS chamber was in the low 10^{-7} to high 10^{-8} Torr range. Additional details of the QMS reactor have been reported previously. ¹⁶

2.2. Chemicals for Ligand-Exchange Reactions. Metal fluoride powders used in the ligand-exchange reactions included GaF_3 (anhydrous, 99.85%, Alfa Aesar), InF_3 (\geq 99.9%, Sigma-Aldrich), ZnF_2 (anhydrous, 99%, Strem Chemicals), ZrF_4 (99.9%, Sigma-Aldrich), HfF_4 (99.9%, Sigma-Aldrich), and SnF_4 (Sigma-Aldrich). The masses of the metal fluoride powders placed in the sample housing were between 0.05 and 0.10 g.

The silane precursors for ligand exchange included both homoleptic and heteroleptic silane precursors. The homoleptic silane precursors were SiCl₄ (99%, Sigma-Aldrich) and Si(CH₃)₄ (99+%, Gelest). The heteroleptic silane precursors were SiCl₂(CH₃)₂ (≥99.5%, Sigma-Aldrich) and SiCl(CH₃)₂H (98%, Sigma-Aldrich). The silane precursors were employed at room temperature. The partial pressures of the silane precursors in the sample housing ranged from 0.05 to 0.20 Torr. These pressures were present continuously during the temperature ramps.

In addition to their ability to perform ligand-exchange reactions, the various silane precursors could be employed for chemical vapor deposition (CVD) at higher temperatures. For example, SiCl together with H₂ can be used for Si CVD at >800 °C. 17,18 Chloromethylsilanes like SiCl (CH 3) can be utilized for SiC CVD at >1200 °C. 19 There have also been reports for thermal pyrolysis of SiCl (CH 3) 2 at >1000 °C. 20 These possible reactions are unlikely at the lower temperatures explored for ligand exchange. The QMS analysis also observed no evidence for products from CVD or thermal pyrolysis reactions at the temperatures < 530 °C employed for ligand exchange.

2.3. Computational Details. The thermodynamics of sequential ligand exchanges between the silane precursors and the metal fluorides was calculated using *ab initio* methods. Geometries and harmonic vibrational frequencies were calculated at the UB3LYP/Def2TZVP level of theory. These calculations were followed by single-point energy calculations at a higher level of theory, UCCSD/sdd. ^{23–25}

Translational, vibrational, and rotational degrees of freedom, along with UCCSD single-point energies, were used to calculate the Gibbs free energies at 350 °C. An in-depth discussion of these thermochemical methods has been described earlier. Gaussian 16 was used for all quantum chemical calculations. Optimizations were performed with Gaussian's opt = tight, enforcing a root mean squared force criterion within 10-6 au. All geometries used in this work were optimized within 100 cycles.

 ΔG was computed using $\Delta G = \Delta H - T\Delta S$. ΔH was calculated as the difference between the enthalpy of the product, $[H(T) - H(0)]_{prod}$ and the enthalpy of the reactant, $[H(T) - H(0)]_{reac}$. H(0) is the enthalpy at zero temperature. [H(T) - H(0)] is calculated using the expression

$$[H(T) - H(0)]_{\text{reac/prod}} = \frac{5}{2} k_{\text{B}} T + \sum_{v_{i}} \frac{h v_{i}}{\exp\left(\frac{h v_{i}}{k_{\text{B}} T}\right) - 1} + \frac{3}{2} k_{\text{B}} T$$
(1)

The translational, vibrational, and rotational contributions are represented by the three terms, respectively, in eq 1. All three terms include the Boltzmann constant, $k_{\rm B}$, and temperature, T. The vibrational term contains contributions from all vibrational frequencies, v_i , that are obtained using UB3LYP/Def2TZVP calculations, and h is Planck's constant.

The entropies of the product, $S_{\rm prod}$, and the reactant, $S_{\rm reac}$ are similarly calculated using

$$S_{\text{reac/prod}} = \frac{\ddot{A}}{k_{\text{B}}} \ln \frac{\dot{i}_{1} 2_{\pi} m k_{\text{B}} T}{\dot{k}_{\text{B}}} \frac{\dot{y}^{3/2}}{k_{\text{B}}} \frac{\dot{y}^{5/2}}{k_{\text{B}}} \frac{\dot{f}_{1}}{k_{\text{B}}} + \sum_{i,j} \frac{\ddot{A}}{k_{\text{B}}} \ln \frac{\dot{i}_{1}}{k_{\text{B}}} - \exp - \frac{\dot{i}_{1} h_{i,j}}{k_{\text{B}} T} \frac{\dot{y}}{k_{\text{B}}} \frac{\dot{y}}{k_{\text{B}}} \frac{\dot{y}^{3/2}}{k_{\text{B}}} + \frac{h_{i,j}}{K_{\text{B}}} \frac{\dot{y}^{3/2}}{k_{\text{B}}} \ln \frac{\dot{i}_{1} \sqrt{\pi}}{k_{\text{B}} T} \prod_{i} \frac{8\pi^{2} l_{i} k_{\text{B}} T}{k_{\text{B}}} \frac{\dot{y}^{3/2} \dot{f}}{k_{\text{B}}} \frac{\dot{f}_{1}}{k_{\text{B}}} \frac{\dot{y}^{3/2}}{k_{\text{B}}} \frac{\dot{f}_{1}}{k_{\text{B}}} \frac{\dot{g}_{1}}{k_{\text{B}}} \frac{\dot{g$$

The translational, vibrational, and rotational contributions are separated as the first, second, and third terms, respectively, in eq 2. m is the mass of the species in question, V is the volume, $\sigma_{\rm ext}$ represents the molecule's external symmetry number, and the principle moments of inertia are given as I_i .

3. RESULTS AND DISCUSSION

3.1. Homoleptic SiCl₄ Precursor with Only Cl Ligands. SiCl₄ (silicon tetrachloride) is a homoleptic silane precursor that is ideal for the study of F/Cl ligand exchange between Cl in SiCl₄ and F in metal fluorides. In addition, SiCl₄ has been used previously as a ligand-exchange precursor for the thermal ALE of ZrO₂ and HfO₂.⁸

3.1.A. GaF_3 . GaF_3 powder was chosen to model Ga_2O_3 after fluorination by HF in the surface modification step during thermal ALE.¹³ Ga_2O_3 thermal ALE has been previously reported using HF for fluorination and BCI_3 , $AI(CH_3)_3$, $AICI(CH_3)_2$, and $Ga(N(CH_3)_2)_3$ as ligand-exchange precursors for volatile release.¹³ There have been no reports of Ga_2O_3 thermal ALE using $SiCI_4$ as the ligand-exchange precursor.

During SiCl₄ exposure to the GaF₃ powder at 375 °C, QMS measurements displayed in Figure 2 observed ion intensities

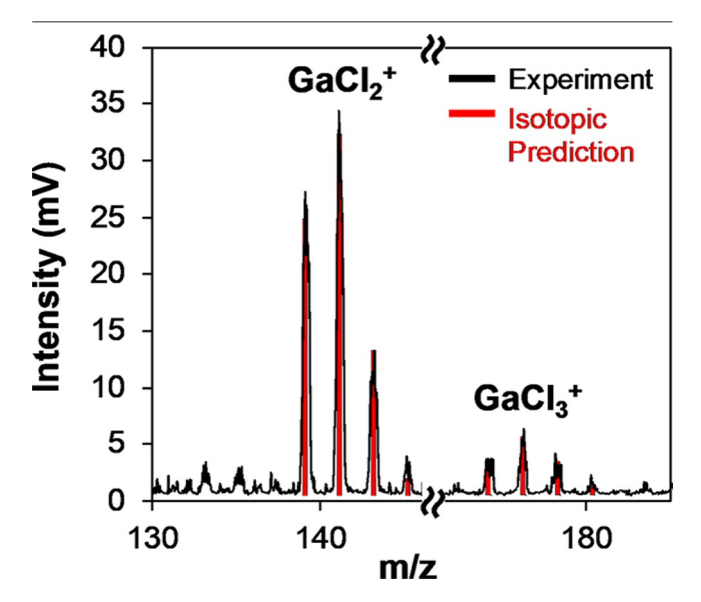


Figure 2. Mass spectrum showing ion intensities of ${\rm GaCl_3}^+$ and ${\rm GaCl_2}^+$ during the ligand-exchange reaction between ${\rm SiCl_4}$ and ${\rm GaF_3}$ powder at 375 °C.

for $GaCl_3^+$ at m/z values of 174, 176, 178, and 180. Under electron impact ionization, $GaCl_3$ also fragmented into $GaCl_3^+$ with ion intensities at m/z values of 139, 141, 143, and 145. These species were identified by the isotopic fingerprints of ^{69}Ga , ^{71}Ga , ^{35}Cl , and ^{37}Cl . The isotopic prediction and experimental mass spectrum are in excellent agreement as depicted in Figure 2. The full mass spectrum from m/z 80–190 is given in Figure S1 in the Supporting Information. The

observation of ${\rm GaCl_3}^+$ in the gas phase indicates complete F/Cl exchange between ${\rm SiCl_4}$ and ${\rm GaF_3}$ to produce ${\rm GaCl_3}$ as a volatile etch product. The observation of ${\rm GaCl_3}$ indicates that the thermal ALE of ${\rm Ga_2O_3}$ should be possible using HF for fluorination and ${\rm SiCl_4}$ as the ligand-exchange precursor for volatile release.

The temperature dependence of the reaction between SiCl $_4$ and ${\rm GaF_3}$ powder is shown in Figure 3. The ${\rm SiCl_3}^+$ ion signal in

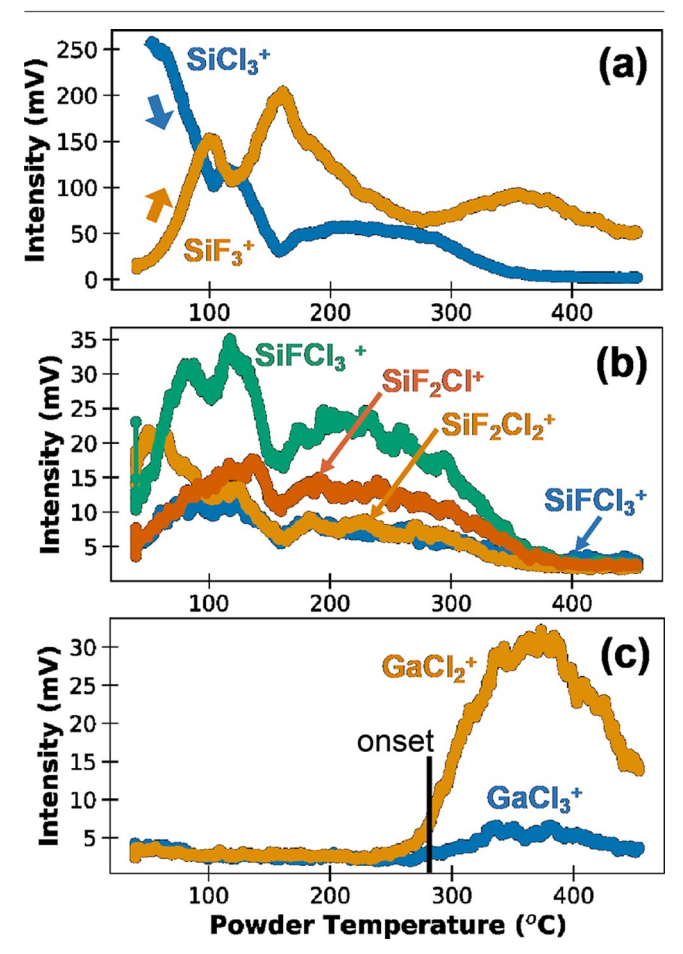


Figure 3. Ion intensities versus powder temperature during reaction between SiCl_4 and GaF_3 powder. (a) SiCl_4 precursor (SiCl_3^+) and SiF_4 ligand-exchange product (SiF_3^+) after complete F/Cl exchange. (b) Various $\operatorname{SiF}_x\operatorname{Cl}_y^+$ species from partial F/Cl exchange. (c) GaCl_3 metal etch product (GaCl_3^+) and its fragment GaCl_2^+ . The most intense isotope peak of each ion species is utilized in the plots.

Figure 3a is the largest signal after ionization of the SiCl $_4$ precursor. ²⁹ As the temperature increased during the temperature ramp, the SiCl $_3$ + ion intensity was observed to decrease progressively. Concurrently, the SiF $_3$ + ion signal increased and exhibited a complementary behavior to the SiCl $_3$ + ion signal. SiF $_3$ + is the main ion signal after ionization of SiF $_4$. ³⁰ Total F/Cl exchange between the SiCl $_4$ precursor and the GaF $_3$ surface produces SiF $_4$. Furthermore, the reciprocal relationship between the SiCl $_3$ + and SiF $_3$ + ion signals indicates that the dominant reaction pathway is complete F/Cl exchange.

Figure 3b shows that partial F/Cl exchange was also observed between SiCl_4 and the GaF_3 powder. However, the ion intensities for the various $\operatorname{SiF}_x\operatorname{Cl}_y^+$ species are much lower than for SiF_3^+ in Figure 3a. The $\operatorname{SiF}_x\operatorname{Cl}_y^+$ ion signals had a maximum intensity of 35 mV. In contrast, the SiF_3^+ ion signal

had a maximum intensity of 200 mV. In addition, the ${\rm SiF_xCl_y}^+$ ion signals did not exhibit a strong correlation with the ${\rm SiCl_3}^+$ ion signal.

Figure 3c shows the results for the GaCl₂⁺ and GaCl₃⁺ ion intensities at *m/z* values of 141 and 176, respectively. These signals are from GaCl₃, the volatile metal etch product.²⁸ The presence of GaCl₃ indicates full F/Cl exchange. The GaCl₃⁺ and GaCl₂⁺ ion signals had an onset temperature of 285 °C. The onset temperature is the lowest temperature where the correct isotopic fingerprints are first observed for a given etch species. In comparison, the SiF₃⁺ ion intensity was observed at temperatures as low as 55 °C. These results illustrate that ligand-exchange products can be observed at a much lower temperature than the metal etch products. Similar observations for ligand exchange with metal fluorides occurring at lower temperatures than the volatile metal etch products were reported earlier.¹⁶

These results suggest that F/Cl exchange leads to the buildup of Cl in the ${\rm GaF_3}$ powder. A certain amount of Cl may be required in the ${\rm GaF_3}$ powder before ${\rm GaCl_3}$ can be released to the gas phase. ${\rm GaCl_3}$ has a vapor pressure of 0.1 Torr at 25 °C. 31 If ${\rm GaCl_3}$ was formed earlier during the temperature ramp, ${\rm GaCl_3}$ should be desorbed and observed at temperatures below its onset temperature at 285 °C. During thermal ALE of ${\rm Ga_2O_3}$ or ${\rm GaN}$, the metal fluoride would only exist on the surface of ${\rm Ga_2O_3}$ or ${\rm GaN}$. The Cl from ligand exchange would not be diluted in a reservoir of metal fluoride. Consequently, the ${\rm GaCl_3}$ etch products should appear at a lower onset temperature than in these experiments on metal fluoride powders.

3.1.B. ZnF₂. ZnF₂ powder models the fluorinated ZnO surface during thermal ALE.³² ZnO thermal ALE has been previously reported using HF for fluorination and Al(CH₃)₃ as the ligand-exchange precursor for volatile release.³² There have been no reports of ZnO thermal ALE using SiCl₄ as the ligand-exchange precursor. The reaction between SiCl₄ and ZnF₂ powder at 475 °C produced ZnCl₂⁺ ion signals as displayed in Figure 4. ZnCl₂⁺ is the parent molecular ion of ZnCl₂.³³ The appearance of ZnCl₂⁺ ion signals indicates F/Cl exchange between the SiCl₄ precursor and the ZnF₂ surface. The

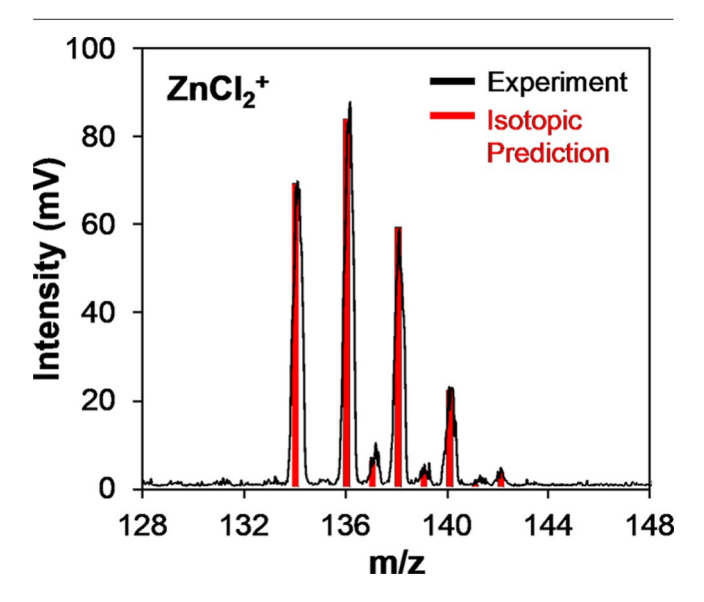


Figure 4. Mass spectrum showing ion intensities of ZnCl₂⁺ during the ligand-exchange reaction between SiCl₄ and ZnF₂ powder at 475 °C.

isotopic prediction (red lines) shown in Figure 4 has an excellent match to the experimental mass spectrum of $\rm ZnCl_2$ at $\it m/z$ values of 134–143 amu. The full mass spectrum from $\it m/z$ 60–150 is given in Figure S2 in the Supporting Information. The observation of $\rm ZnCl_2^+$ ion intensity suggests that $\rm ZnO$ thermal ALE using HF for fluorination and $\rm SiCl_4$ for volatile release should be feasible.

The temperature dependence of the reaction between $SiCl_4$ and ZnF_2 powder is shown in Figure 5. As the $SiCl_3^+$ ion

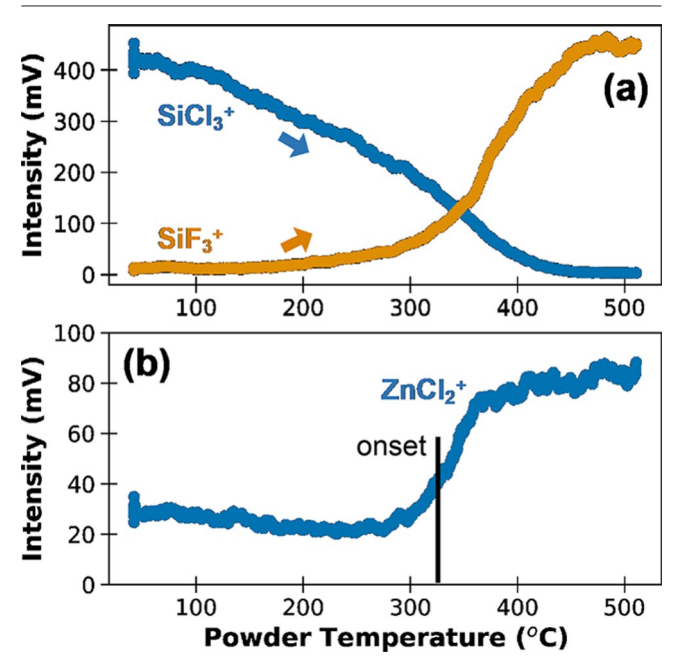


Figure 5. Ion intensities versus powder temperature during the reaction between SiCl_4 and ZnF_2 powder. (a) SiCl_4 precursor (SiCl_3^+) and SiF_4 ligand-exchange product (SiF_3^+) after total F/Cl exchange. (b) ZnCl_2 metal etch product (ZnCl_2^+). The most intense isotope peak of each ion species is shown in the plots.

intensity decreased progressively with temperature in Figure 5a, the ${\rm SiF_3}^+$ ion intensity increased in a complementary fashion with an onset temperature of 250 °C. This behavior demonstrates F/Cl exchange between ${\rm SiCl}_4$ and ${\rm ZnF}_2$ Figure 5b shows that the ${\rm ZnCl}_2^+$ ion signal, representing the metal etch product, has an onset temperature at 325 °C. The observation of ${\rm ZnCl}_2^+$ ion signal at only a slightly higher temperature than the onset temperature for ligand exchange indicates that F/Cl exchange readily forms a volatile ${\rm ZnCl}_2$ etch product.

3.1.C. ZrF_4 ZrF_4 powder models the fluorinated ZrO_2 surface in thermal ALE. ZrO_2 thermal ALE has been previously reported using HF for fluorination and AlCI(CH $_3$) $_2$ SiCI $_4$ and TiCI $_4$ as the ligand-exchange precursors for volatile release. $^{6-8}$ Various ion signals containing Zr were observed during SiCI $_4$ exposure to ZrF_4 powder at 450 °C. Figure 6 shows the most intense ion signals assigned to $ZrFCI_3^+$ based on the characteristic combinations of Zr, Zr, and Zr isotopes.

The ${\sf ZrFCl_3}^+$ ion signal is the result of three F/Cl exchanges between ${\sf SiCl_4}$ and ${\sf ZrF_4}$. The observation of ${\sf ZrFCl_3}^+$ indicates that complete F/Cl exchange to ${\sf ZrCl_4}$ is not necessary for volatile release of a ${\sf Zr-containing}$ species. The QMS analysis also observed smaller ion signals for ${\sf ZrCl_4}^+$ resulting from four F/Cl exchanges and ${\sf ZrF_2Cl_2}^+$ resulting from two F/Cl

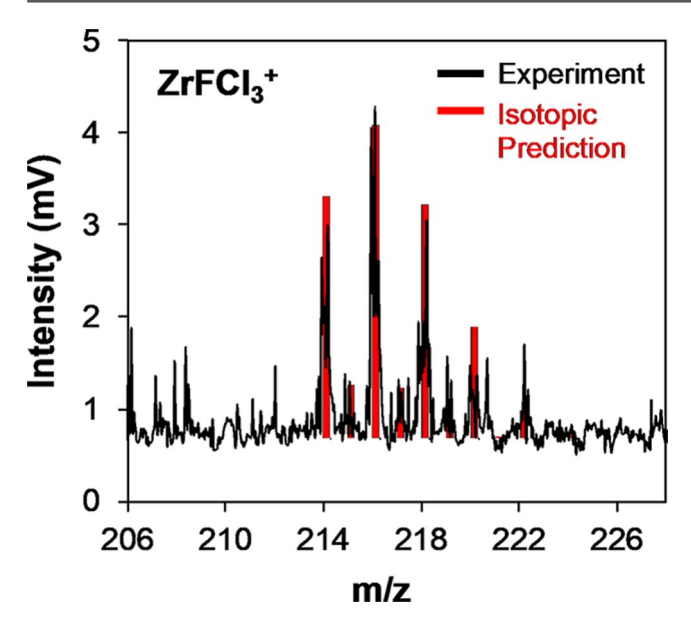


Figure 6. Mass spectrum showing ion intensities of $\rm ZrFCl_3^+$ during the ligand-exchange reaction between $\rm SiCl_4$ and $\rm ZrF_4$ powder at 450 °C.

exchanges. The full mass spectrum from m/z 80–230 is given in Figure S3 in the Supporting Information.

The temperature dependence of the reaction between $SiCl_4$ and ZrF_4 powder is displayed in Figure 7. The reciprocal

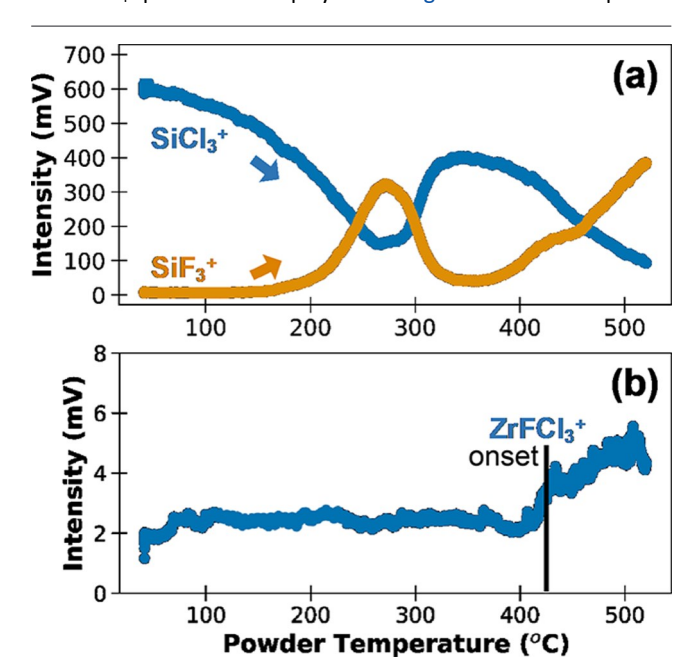


Figure 7. Ion intensities versus powder temperature during the reaction between SiCl_4 and ZrF_4 powder. (a) SiCl_4 precursor (SiCl_3^+) and SiF_4 ligand-exchange product (SiF_3^+) after total F/Cl exchange. (b) ZrFCl_3 metal etch product (ZrFCl_3^+).

relationship between the $\mathrm{SiCl_3}^+$ and $\mathrm{SiF_3}^+$ ion intensities is shown in Figure 7a. The ion intensity for $\mathrm{SiCl_3}^+$ decreases as the ion intensity of $\mathrm{SiF_3}^+$ increases from 175 to 275 °C. The ion intensity for $\mathrm{SiCl_3}^+$ then increases as the ion intensity of $\mathrm{SiF_3}^+$ decreases from 275 to 350 °C. Lastly, the ion intensity for $\mathrm{SiCl_3}^+$ decreases as the ion intensity of $\mathrm{SiF_3}^+$ increases from 350 to 530 °C. This complementary behavior argues for full F/

CI exchange for ${\rm SiCl}_4$ in its reaction with ${\rm ZrF}_4$ powder throughout the entire temperature range.

The correlated increases and decreases in the ion intensities for SiCl₃⁺ and SiF₃⁺ in Figure 7a can be interpreted in terms of the buildup of chlorine on the ZrF₄ powder. As the chlorine coverage increases on the metal fluoride surface, less fluorine species are available for ligand exchange. This chlorine buildup could explain the decrease of the SiF ⁺₃ ligand-exchange product from 275 to 350 °C. The ZrFCl₃ metal chloride etch products then are desorbed at >400 °C as shown in Figure 7b. As chlorine is lost from the metal fluoride powder, more fluorine surface species are available and ligand exchange can again convert the SiCl₄ precursor to the SiF₄ ligand-exchange product.

The onset temperature for F/Cl exchange as measured by the appearance of the SiF₃⁺ ion signal in Figure 7a is 175 °C. In contrast, Figure 7b shows that the ion intensity for ZrFCl₃⁺, from the main metal etch product, was not observed until 425 °C. ZrCl₄ can be used as a proxy for ZrFCl₃, ZrCl₄ exhibits a high vapor pressure of 0.51 Torr at 175 °C and 1240 Torr at 350 °C.³⁴ Therefore, ZrFCl₃ is expected to desorb if ZrFCl₃ is formed at the onset for ligand exchange at 175 °C. The expected ZrFCl₃ vapor pressure cannot explain the large temperature difference between the appearance of ligand-exchange products and metal etching products.

The measured ZrFCl₃⁺ ion signals were also low. SiF₃⁺ ion signals were measured with intensities as high as 400 mV in Figure 6a. In contrast, the ZrFCl₃⁺ ion signals observed in Figure 6b were only around 1% of the SiF₃⁺ ion signals in Figure 7a. The low signals of the Zr-containing etch products may result from lower ionization cross sections. In addition, the low signals could be due to a dilution effect. As F/Cl exchange occurs between the SiCl₄ precursor and the ZrF₄ surface, the Cl ligands initially exchanged with ZrF₄ on the surface could be diluted in the underlying ZrF₄ powder. Because of this dilution, volatile ZrF_xCl_y⁺ species may not be detected until higher temperatures after enough Cl has built up in the ZrF₄ powder.

3.1.D. InF₃, HfF₄, and SnF₄. Similar experiments were conducted using InF₃, HfF₄, and SnF₄ powders. The temperature dependence of the reaction of SiCl₄ with InF₃ and HfF₄ powder was reported earlier. The temperature dependence of the reaction of SiCl₄ with SnF₄ powder is presented in the Supporting Information in Figure S4.

3.2. Heteroleptic $SiCl_2(CH_3)_2$ Precursor with CI and CH₃ Ligands. $SiCl_2(CH_3)_2$ (dichlorodimethyl-silane) is a heteroleptic silane precursor that contains both CI and CH₃ ligands. $SiCl_2(CH_3)_2$ can be employed to determine the relative rates between F/CI and F/CH₃ ligand exchange. $SiCl_2(CH_3)_2$ has not been used as a ligand-exchange precursor for thermal ALE.

3.2.A. GaF_3 . The reaction of $SiCl_2(CH_3)_2$ with GaF_3 powder resulted in the observation of $GaCl_2^+$ and $GaCl_3^+$ ion signals as the metal etch products, similar to the reaction of $SiCl_4$ with GaF_3 powder displayed in Figure 2. These CI-containing metal etch products indicate that F/CI ligand exchange dominates over F/CH_3 ligand exchange. Temperature-dependent results for the reaction between $SiCl_2(CH_3)_2$ and GaF_3 powder are presented in Figure 8.

Figure 8a shows the ion signals for $SiCl_2(CH_3)^+$, the main ion signal from the $SiCl_2(CH_3)_2$ precursor, and $SiF_2(CH_3)^+$, the main ion signal from the $SiF_2(CH_3)_2$ ligand-exchange product.³⁵ The decreases and increases of the $SiCl_2(CH_3)^+$ and

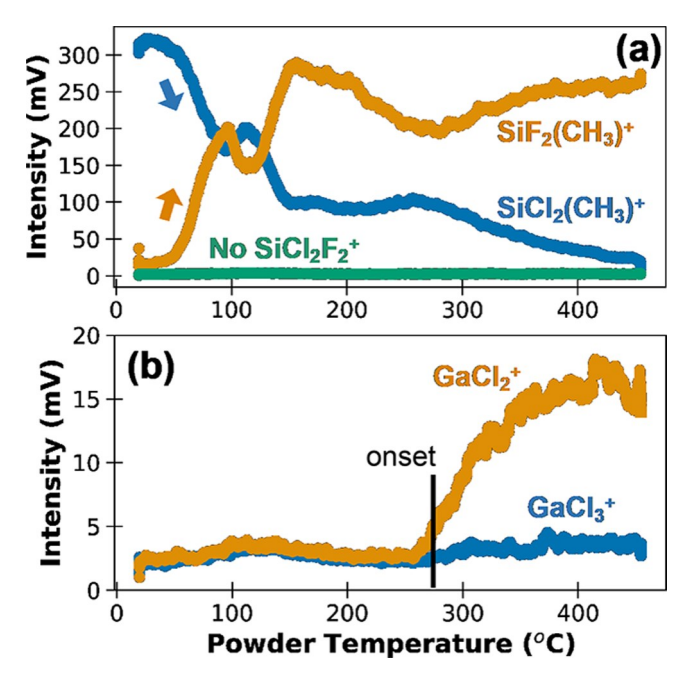


Figure 8. Ion intensities versus powder temperature during the reaction between $SiCl_2(CH_3)_2$ and GaF_3 powder. (a) $SiCl_2(CH_3)_2$ precursor $(SiCl_2(CH_3)^+)$, $SiF_2(CH_3)_2$ ligand-exchange product $(SiF_2(CH_3)^+)$, and possible $SiCl_2F_2$ ligand-exchange product after complete F/CH_3 exchange $(SiCl_2F_2^+)$. (b) $GaCl_3$ metal etch product $(GaCl_3^+)$ and its fragment $GaCl_2^+$.

 $\operatorname{SiF}_2(\operatorname{CH}_3)^+$ ion signals are correlated with each other. This complementary behavior argues that complete F/CI ligand exchange is the dominant ligand-exchange reaction throughout the temperature ramp. The complementary behavior may be partially explained by the buildup of chlorine on the GaF_3 surface. When the GaCI_3 desorbs at >275 °C, more fluorine species are available for ligand exchange and the $\operatorname{SiF}_2(\operatorname{CH}_3)^+$ ion signal increases and the $\operatorname{SiCI}_2(\operatorname{CH}_3)^+$ ion signal decreases.

There is no evidence for any F/CH_3 ligand exchange from the ligand-exchange products. For example, the baseline intensity of $SiCl_2F_2^+$ in Figure 8a demonstrates the lack of products from total F/CH_3 exchange. Furthermore, products indicative of partial F/CH_3 exchange were also not observed such as $SiCl_2(CH_3)F^+$ and its possible fragments. $Ga(CH_3)_3$ and its fragments were also not produced resulting from the lack of F/CH_3 exchange.

The ion signals for the metal etch products are displayed in Figure 8b. These ion intensities are consistent with the electron impact ionization of ${\rm GaCl_3}^{28}$ The results for the ${\rm GaCl_2}^+$ and ${\rm GaCl_3}^+$ ion intensities are also very similar in Figure 8b and Figure 3c. This similarity between ${\rm SiCl_2}({\rm CH_3})_2$ in Figure 8b and ${\rm SiCl_4}$ in Figure 3c argues that F/Cl is the main ligand-exchange reaction.

3.2.B. ZnF_2 . The reaction between $SiCl_2(CH_3)_2$ and ZnF_2 powder produced $ZnCl_2^+$ ion signals from the $ZnCl_2$ metal etch product similar to the reaction of $SiCl_4$ with ZnF_2 powder displayed in Figure 4. These Cl-containing metal etch products again indicate that F/Cl exchange is dominant. Figure 9a shows the temperature dependence of the reaction between $SiCl_2(CH_3)_3$ and ZnF_2 . The correlation between the decrease in the $SiCl_2(CH_3)^+$ ion signal for the precursor and the increase in the $SiF_2(CH_3)^+$ ion signal for the ligand-exchange product in Figure 9a is very complementary and consistent with total F/Cl exchange over the entire temperature ramp.

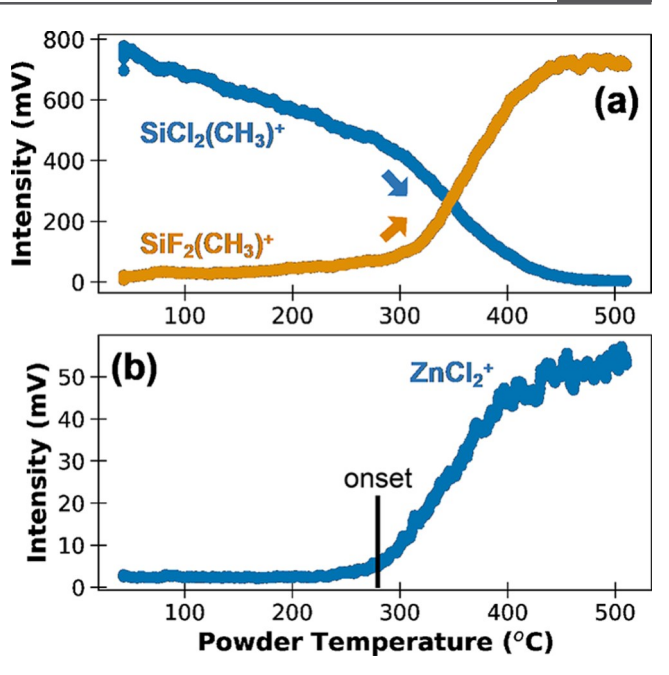


Figure 9. Ion intensities versus powder temperature during the reaction between $SiCl_2(CH_3)_2$ and ZnF_2 powder. (a) $SiCl_2(CH_3)_2$ precursor $(SiCl_2(CH_3)^+)$ and $SiF_2(CH_3)_2$ ligand-exchange product after total F/Cl exchange $(SiF_2(CH_3)^+)$. (b) $ZnCl_2$ metal etch product $(ZnCl_2^+)$.

There is no evidence for any F/CH_3 exchange. The QMS measurements did monitor minor $SiFCI(CH_3)_2^+$ ion signals that arise from partial F/CI exchange. However, these ion signals have intensities < 80 mV and are not shown in Figure 9a.

Figure 9b shows $ZnCl_2$, the dominant metal etch product. No ion signals were observed that were consistent with $Zn(CH_3)_2^+$, $ZnF(CH_3)^+$, or any of their possible fragments. The $ZnCl_2^+$ ion signal was observed with an onset etching temperature of 280 °C. This onset temperature is similar to the onset temperature of 250 °C for the $SiF_2(CH_3)^+$ ion signal resulting from full F/Cl exchange for $SiCl_2(CH_3)_2^-$ in its reaction with ZnF_2 powder. $ZnCl_2$ can desorb nearly as soon as $ZnCl_2^-$ is formed by ligand exchange.

3.2.C. ZrF_4 . The reaction between $SiCl_2(CH_3)_2$ and ZrF_4 powder produced $ZrFCl_3^+$ ion signals from the $ZrFCl_3$ metal etch product similar to the reaction of $SiCl_4$ with ZrF_4 powder displayed in Figure 6. These results again support F/Cl ligand exchange as the sole ligand-exchange reaction. Temperature-dependent results for the reaction between $SiCl_2(CH_3)_2$ and ZrF_4 powder are shown in Figure 10. As expected if F/Cl exchange is the only ligand-exchange reaction, the $SiCl_2(CH_3)^+$ and $SiF_2(CH_3)^+$ ion intensities are highly correlated in Figure 10a. The complementary behavior may be partially explained by the buildup and desorption of chlorine on the ZrF_4 surface.

The F/Cl exchange was observed with an onset temperature at 140 °C as displayed in Figure 10a. However, the $ZrCl_4^+$ and $ZrFCl_3^+$ ion intensities from the Zr-containing etch products were not observed until 375 °C as shown in Figure 10b. The large difference in the onset temperatures for ligand-exchange and metal etch products again suggests that Cl needs to build up in the ZrF_4 powder before $ZrCl_4$ can desorb as a metal etch product. In addition, the large ion signal intensity differences between $SiF_2(CH_3)^+$ and $ZrFCl_3^+$ or $ZrCl_4^+$ suggests that either the Zr-containing etch products have lower ionization

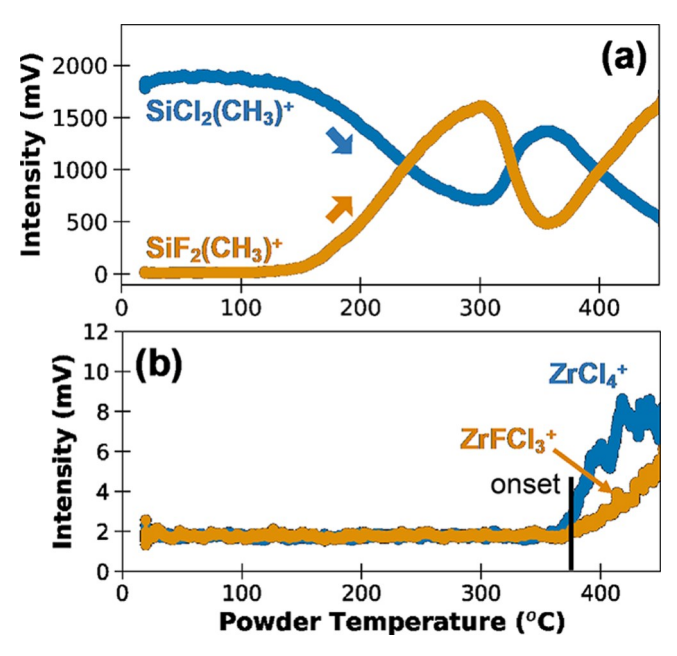


Figure 10. Ion intensities versus powder temperature during the reaction between $SiCl_2(CH_3)_2$ and ZrF_4 powder. (a) $SiCl_2(CH_3)_2$ precursor $(SiCl_2(CH_3)^+)$ and $SiF_2(CH_3)_2$ ligand-exchange product after total F/Cl exchange $(SiF_2(CH_3)^+)$. (b) $ZrCl_4$ and $ZrFCl_3$ metal etch products $(ZrCl_4^+)$ and $ZrFCl_3^+)$.

cross sections or that the CI ligands may be diluted in the ${\rm ZrF}_4$ powder.

There was no evidence for F/CH $_3$ exchange in the ligand-exchange products for the reaction between SiCl $_2$ (CH $_3$) $_2$ and ZrF $_4$ powder. The lack of F/CH $_3$ exchange is consistent with a small Zr-CH $_3$ bond energy and the low decomposition temperature of \leq 15 °C for Zr(CH $_3$) $_4$. The weak Zr-CH $_3$ bond also explained the lack of thermal ZrO $_2$ ALE using HF and Al(CH $_3$) $_3$ as the reactants. 8,37

3.3. Heteroleptic SiCl(CH₃)₂H Precursor with Cl, CH₃ and H Ligands. SiCl(CH₃)₂H (chlorodimethyl-silane) is a heteroleptic precursor. The ligand exchange between SiCl-(CH₃)₂H with metal fluorides could occur with F/Cl, F/CH₃ or F/H exchange. SiCl(CH₃)₂H has not been used as a ligand-exchange precursor for thermal ALE.

3.3.A. GaF_3 . The reaction between $SiCI(CH_3)_2H$ and GaF_3 powder produced $GaCI_2^+$ and $GaCI_3^+$ ion signals similar to the reaction of $SiCI_4$ with GaF_3 powder displayed in Figure 2. Even though CH_3 and H ligands could participate, the CI-containing metal etch products indicate that F/CI ligand exchange is dominant. Figure 11a shows the temperature dependence of the reaction between $SiCI(CH_3)_2H$ and GaF_3 powder. Below 200 °C, there is correlated behavior between the $SiCI(CH_3)_2^+$ ion intensity for the precursor and the $SiF(CH_3)_2^+$ ion intensity for the main ligand-exchange product. The $SiF(CH_3)_2^+$ ion intensity at a m/z value of 93 is attributed to the ionization of $SiF(CH_3)_2H$. This complementary behavior argues for dominant F/CI exchange between $SiCI(CH_3)_2H$ and the GaF_3 powder. In addition, the F/CI exchange has a low onset temperature of 60 °C.

Figure 11b shows the ion intensities for the species that result from F/H exchange. The $SiF_2(CH_3)_2^+$ ion intensity indicates both F/H and F/Cl exchange. The $SiCl(CH_3)F^+$ ion intensity indicates only F/H exchange. However, the $SiF_2(CH_3)_2^+$ and $SiCl(CH_3)F^+$ ion intensities are much lower than the ion intensity for $SiF(CH_3)_2^+$ in Figure 11a.

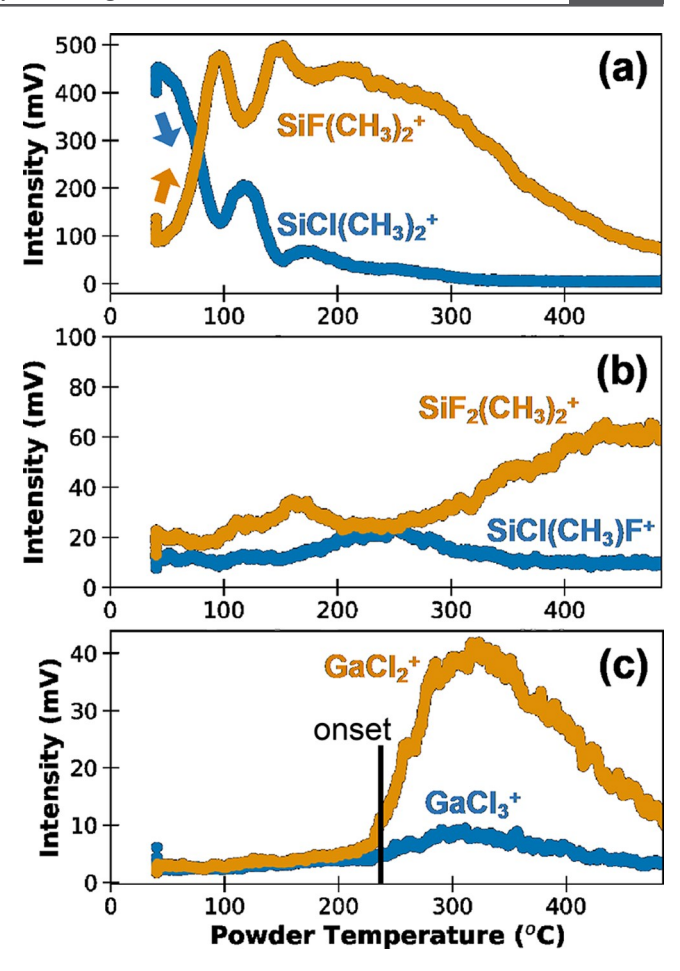


Figure 11. Ion intensities versus powder temperature during the reaction between $SiCI(CH_3)_2H$ and GaF_3 powder. (a) $SiCI(CH_3)_2H$ precursor $(SiCI(CH_3)_2^+)$ and $SiF(CH_3)_2H$ ligand-exchange product after F/CI exchange $(SiF(CH_3)_2^+)$. (b) $SiCI(CH_3)_2F$ ligand-exchange product after F/H exchange $(SiCI(CH_3)_2F^+)$ and $SiF_2(CH_3)_2$ ligand-exchange product after both F/CI and F/H exchange $(SiF_2(CH_3)_2^+)$. (c) $GaCI_3$ metal etch product $(GaCI_3^+)$ and its fragment $GaCI_2^+$.

The onset temperature for the $SiF_2(CH_3)_2^+$ ion intensity resulting from both F/H and F/Cl exchange is observed at 350 °C. This onset temperature is much higher than the onset temperature of 60 °C for the $SiF(CH_3)_2^+$ ion intensity resulting from F/Cl exchange.

Figure 11c shows that the ${\rm GaCl_3}^+$ ion intensity for the metal etch product has an onset temperature of 240 °C. This onset temperature is much higher than the onset temperature of 60 °C for F/Cl exchange in Figure 11a. This difference again argues that Cl must be building up in the ${\rm GaF_3}$ powder prior to the desorption of ${\rm GaCl_3}$ at 240 °C. There is also a similarity between the onset temperatures for the observation of ${\rm GaCl_2}^+$ and ${\rm GaCl_3}^+$ ion intensities during the reaction of ${\rm SiCl_4}$, ${\rm SiCl_2(CH_3)_2}$ and ${\rm SiCl(CH_3)_2H}$ with ${\rm GaF_3}$ powder in Figures 3c, 8b and 11c. Independent of the exact nature of the silane, the presence of Cl ligands and F/Cl exchange are the most important factors for the ligand-exchange reaction.

3.3.B. ZnF_2 . For the reaction of the heteroleptic SiCI-(CH $_2$) $_2$ H precursor with ZnF_2 powder, $ZnCI_2$ + ion signals were detected as the metal etch products similar to the reaction of SiCI $_4$ with ZnF_2 powder shown in Figure 4. The CI-containing metal etch products indicate that F/CI ligand exchange is dominant. Figure 12a shows the temperature dependence of

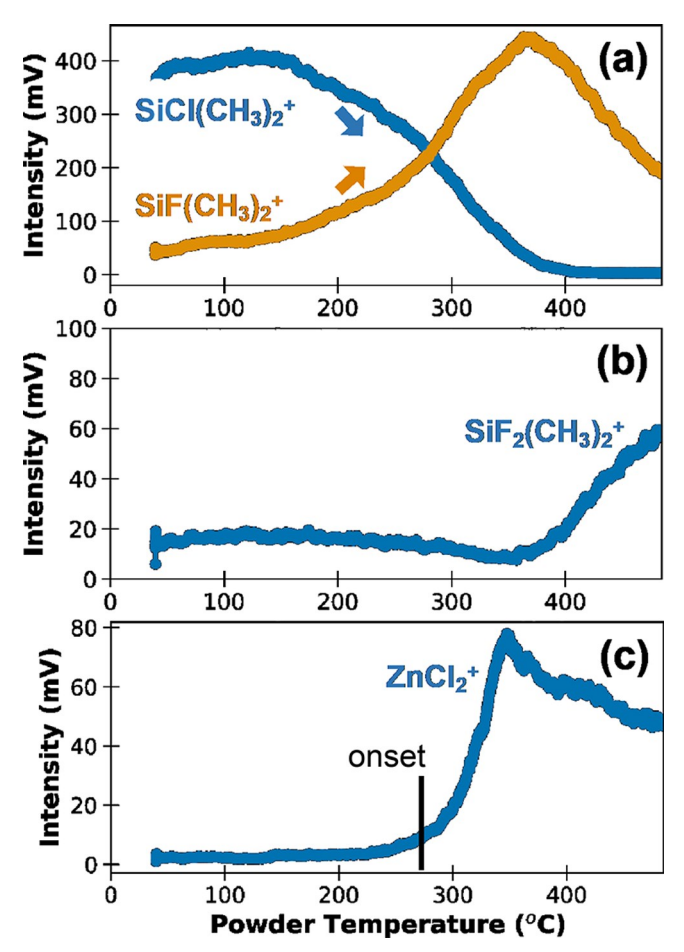


Figure 12. Ion intensities versus powder temperature during the reaction between $SiCI(CH_3)_2H$ and ZnF_2 powder. (a) $SiCI(CH_3)_2H$ precursor $(SiCI(CH_3)_2^+)$ and $SiF(CH_3)_2H$ ligand-exchange product after F/CI exchange $(SiF(CH_3)_2^+)$. (b) $SiF_2(CH_3)_2$ ligand-exchange product after both F/CI and F/H exchange $(SiF_2(CH_3)_2)^+$. (c) $ZnCI_2$ metal etch product $(ZnCI_2^+)$.

the reaction between $SiCI(CH_3)_2H$ and ZnF_2 powder. The $SiCI(CH_3)_2^+$ ion intensity decreases in conjunction with the increase in the $SiF(CH_3)_2^+$ ion intensity. This ligand-exchange product results from F/CI exchange as expected from the observation of $ZnCI_2^+$ as the metal etch product. The onset temperature for the $SiF(CH_3)_2^+$ ion intensity is 180 °C.

The complementary behavior between the $SiCl(CH_3)_2^+$ and $SiF(CH_3)_2^+$ ion intensities is lost at >370 °C when the $SiF(CH_3)_2^+$ ion intensity decreases with no corresponding rise in the $SiCl(CH_3)_2^+$ ion intensity. This change results from the rise of the $SiF_2(CH_3)_2^+$ ion intensity shown in Figure 12b. The $SiF_2(CH_3)_2^+$ ion intensity results from both F/Cl and F/H exchange between $SiCl(CH_3)_2^+$ and the ZnF_2 powder. This observation indicates that F/H exchange becomes competitive with F/Cl exchange at higher temperatures.

Figure 12c shows that $ZnCl_2$ is observed as the main metal etch product. The $ZnCl_2^+$ ion signals have an onset temperature at 275 °C. This onset temperature is higher than the onset temperature for F/Cl exchange at 180 °C. The Cl ligands are building up prior to the desorption of $ZnCl_2$ at \geq 275 °C. In addition, there is a similarity between the onset temperatures for the $ZnCl_2^+$ ion intensity for the reaction of $SiCl_4$, $SiCl_2(CH_3)_2$ and $SiCl(CH_3)_2H$ with ZnF_2 powder in Figures 5b, 9b, and 12c. This behavior again demonstrates that

F/Cl exchange is the dominant ligand-exchange pathway for all the silane precursors.

3.3.C. ZrF₄. For the reaction of SiCI(CH₃)₂H with ZrF₄ powder, ZrFCI₃⁺ ion signals were detected as the metal etch products similar to the reaction of SiCI₄ with ZrF₄ powder shown in Figure 6. The Cl-containing metal etch products argue that F/CI ligand exchange is the dominant ligand-exchange pathway. Ligand exchange with CH₃ and H ligands is not occurring during the reaction of SiCI(CH₃)₂H with ZrF₄ powder.

In support of F/Cl ligand exchange, Figure 13a shows remarkably complementary behavior between the SiCl(CH₃)₂⁺

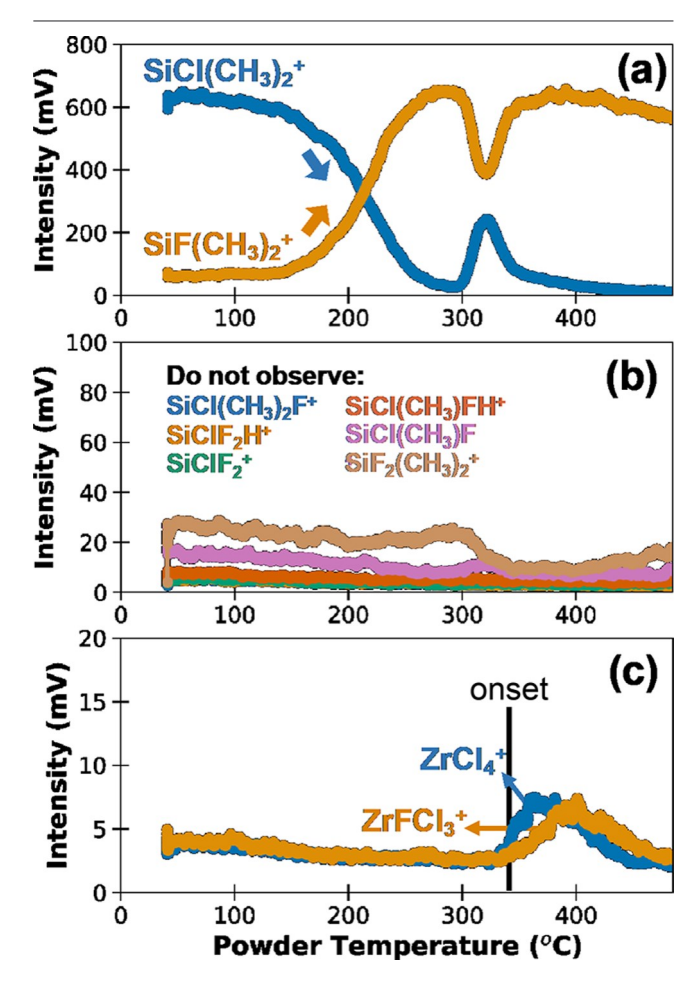


Figure 13. Ion intensities versus powder temperature during the reaction between $SiCI(CH_3)_2H$ and ZrF_4 powder. (a) $SiCI(CH_3)_2H$ precursor $(SiCI(CH_3)_2^+)$ and $SiF(CH_3)_2H$ ligand-exchange product after F/CI exchange ($SiF(CH_3)_2^+$). (b) $SiCI(CH_3)_2H$ precursor after F/CH₃ or F/H exchange (many possible species, not observed). (c) $ZrCI_4$ and $ZrFCI_3$ metal etch products ($ZrCI_4^+$ and $ZrFCI_3^+$).

ion intensity for the precursor and the $SiF(CH_3)_2^+$ ion intensity for the main ligand-exchange product. The SiCI-(CH $_3$) $_2^+$ and $SiF(CH_3$) $_2^+$ ion intensities in Figure 13a form near mirror images of each other. The prominent decrease/increase of the $SiF(CH_3)_2^+/SiCI(CH_3)_2^+$ signals from 300 to 325 °C and the subsequent increase/decrease of the $SiF(CH_3)_2^+/SiCI(CH_3)_2^+$ signals from 325 to 350 °C correlate with the onset of $ZrFCI_3$ and $ZrCI_4$ desorption at 325 °C. The buildup of chlorine can decrease the ligand-exchange reaction. The loss of chlorine by metal chloride desorption can then increase the ligand-exchange reaction.

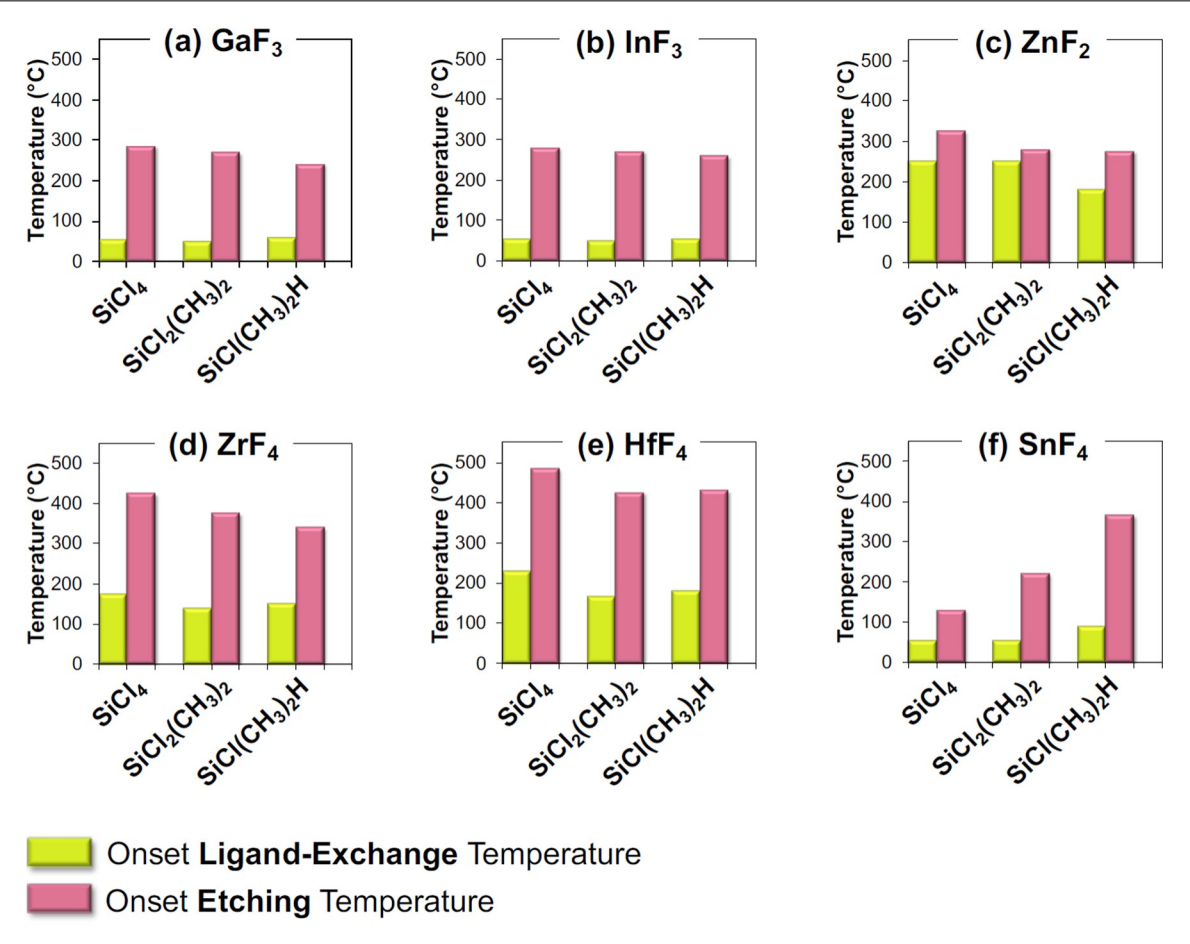


Figure 14. Onset temperatures for ligand exchange and metal etching observed for spontaneous etching of various metal fluorides (GaF 3 InF 3 ZnF2, ZrF4, HfF4, and SnF4) using different silane precursors (SiCl4, SiCl2(CH3)2, and SiCl(CH3)2H).

There are also no species observed from possible F/CH $_3$ or F/H exchange. All of the species that may result from F/CH $_3$ or F/H exchange are shown in Figure 13b. All of these species are negligible. Due to the dominant F/CI exchange, the metal etch products produced ${\rm ZrF}_x{\rm CI}_y^+$ ion species as displayed in Figure 13c. The ${\rm ZrCI}_4^+$ and ${\rm ZrFCI}_3^+$ ion signals provide evidence for both complete and partial F/CI exchange between the ${\rm SiCI}({\rm CH}_3)_2{\rm H}$ precursor and the ${\rm ZrF}_4$ powder. The Zrcontaining etch products have an onset temperature of 340 °C. This onset temperature is much higher than the onset temperature of 150 °C for F/CI exchange. This temperature difference again indicates that CI buildup in the ${\rm ZrF}_4$ powder may be required for volatile release of the Zr-containing etch products.

The low intensities of the Zr-containing etch products observed in Figure 13c may result from low ionization eficiencies or a dilution effect as suggested earlier. There is also a similarity between the onset temperatures for the $\rm ZrFCl_3^+$ and $\rm ZrCl_4^+$ ion intensities for the reactions of $\rm SiCl_4$, $\rm SiCl_2(CH_3)_2$ and $\rm SiCl(CH_3)_2H$ with $\rm ZrF_4$ powder in Figures 7b, 10b and 13c. This similarity again argues that F/Cl exchange is the main ligand-exchange pathway.

3.4. Homoleptic $Si(CH_3)_4$ Precursor with Only CH_3 Ligands. $Si(CH_3)_4$ (tetramethyl-silane) is a homoleptic silane precursor that only contains CH_3 ligands. In the absence of CI ligands, $Si(CH_3)_4$ can test if F/CH_3 exchange is possible when F/CH_3 exchange is the only option. In all cases, no ligand-exchange products or metal etch products were observed for the reaction of $Si(CH_3)_4$ with any of the metal fluorides. These

experiments confirm that F/CH_3 exchange is not favorable even in the absence of CI ligands.

3.5. Onset Temperatures for Ligand-Exchange and Etching Reactions. The onset temperatures for ligandexchange and etching reactions for the various silane precursors with all the metal fluorides are shown in Figure 14. The onset temperatures for the various metal fluorides include GaF, ZnF, and ZrF, that have been discussed earlier in this paper. In addition, the onset temperatures are also given for InF , HfF and SnF that were examined using similar experiments. The differences between the metal fluorides reveal the diverse landscape for the spontaneous etching of metal fluorides by silane precursors using ligand-exchange reactions.¹⁶ In some cases, the metal etch products can appear at much higher temperatures than the onset temperature for the ligand-exchange products. The metal etch products can also appear at temperatures that are comparable to the onset temperature for the ligand-exchange products.

 ${\rm GaF_3}$ in Figure 14a and ${\rm InF_3}$ in Figure 14b display similar trends. Both ${\rm GaF_3}$ and ${\rm InF_3}$ are Group 13 metal fluorides. The onset temperatures for ligand exchange are comparable at 50–60 °C. The onset temperatures for metal etching are also comparable at 240–285 °C. Both ${\rm GaF_3}$ and ${\rm InF_3}$ have a large difference between their onset temperatures for ligand-exchange and metal etching reactions. The difference between the two onset temperatures is in the range of 180–230 °C.

Although GaF₃ and InF₃ display comparable behavior in Figure 14a,b, GaCl₃ and InCl₃ have different vapor pressures. GaCl₃ has a vapor pressure of 1 Torr at 48 °C. 31,38 InCl₃ does

not obtain a vapor pressure of 1 Torr until 2350 °C. 39 GaCl should have suficient vapor pressure at ≥ 1 Torr to desorb at or above the onset temperatures for ligand exchange. In contrast, InCl₃ will have a much lower pressure at the onset temperature for ligand-exchange. InCl₃ desorption would not be anticipated until much higher temperatures.

Given that GaCl₃ and InCl₃ have very different vapor pressures, the similarity between parts a and b of Figure 14 must be explained by a different mechanism. The dilution of the CI from F/CI exchange in the metal fluoride could explain the large difference between the onset temperatures for ligand-exchange and metal etch products. Perhaps a critical concentration of CI is required in the metal fluoride prior to desorption of the GaCl₃ or InCl₃ metal etch products.

ZnF₂ in Figure 14c demonstrates the case where the ligand exchange and metal etch products are observed at similar temperatures. The onset temperatures for ligand exchange at between 180 and 250 °C are noticeably higher than for the other metal fluorides. These higher onset temperatures may result from less favorable ligand-exchange reactions with ZnF₂. In comparison, the onset temperatures for metal etch products are between 275 and 325 °C. The resulting difference between the two onset temperatures is only 30–95 °C.

The ZnCl₂ metal etch product resulting from the F/Cl exchange has the lowest vapor pressure of all the various metal chloride etch products. ZnCl₂ has a vapor pressure of only 0.025 Torr at 300 °C⁴⁰ and 1 Torr at 428 °C.³⁸ The similar onset temperatures may indicate that the Cl from ligand exchange forms ZnCl₂ on the surface of the ZnF₂ powder. ZnCl₂ then desorbs only when the temperatures are suficient to sublime ZnCl₂.

ZrF₄ and HfF₄ are Group 4 metal fluorides. ZrF₄ in Figure 14d and HfF₄ in Figure 14e both display a difference between the onset temperatures for ligand-exchange and metal etch products. The onset temperatures for ligand exchange are between 140 and 230 °C. The onset temperatures for metal etching are between 340 and 485 °C. The resulting difference between the two onset temperatures is in the range of 190–260 °C. ZrCl₄ and HfCl₄ both have similar vapor pressures at and above the onset temperatures for ligand exchange. ZrCl₄ has a vapor pressure of 1 Torr at 180 °C. ⁴¹ HfCl₄ has a vapor pressure of 1 Torr at 170 °C. ⁴¹ Similar onset temperatures for the metal etch products are expected if the products have comparable vapor pressures.

The trends for ${\rm SnF_4}$ in Figure 14f are different than the other metal fluorides. For ${\rm SnF_4}$ the onset temperatures for metal etch products exhibit a dependence on the number of CI ligands in the silane precursor. The reaction of ${\rm SiCI_4}$ with ${\rm SnF_4}$ displays an onset temperature for metal etch products at 130 °C. The reaction of ${\rm SiCI_2}({\rm CH_3})_2$ with ${\rm SnF_4}$ displays a higher onset temperature for metal etch products at 220 °C. The reaction of ${\rm SiCI}({\rm CH_3})_2{\rm H}$ with ${\rm SnF_4}$ has an even higher onset temperature for metal etch products at 365 °C. In all cases, F/CI exchange is the ligand-exchange pathway and ${\rm SnCI_4}$ is the exclusive metal etch product.

The very high volatility of SnCl₄ may explain the dependence between the onset temperature for metal etch products and the number of Cl ligands in the silane precursor in Figure 14f. The vapor pressure of SnCl₄ is 26 Torr at room temperature.⁴² With such a high SnCl₄ volatility, SnCl₄ can desorb as a metal etch product as soon as there is sufficient F/Cl exchange between the silane precursor and the SnF₄ powder. Although the SnF₄ onset temperatures scale inversely

with the number of CI ligands in the silicon precursor in Figure 14f, a longer exposure time with a silane with fewer CI ligands may be expected to display a lower onset temperature. Future experiments at different heating rates should be conducted to test this proposition.

3.6. Thermochemical Calculations of Ligand-Exchange Reactions. Successful thermal ALE requires favorable thermodynamics for the modification and volatile release reactions. The favorability of the ligand-exchange reaction can be measured by the change in Gibbs free energy (ΔG) . Figure 15 shows the ΔG values for the ligand-exchange

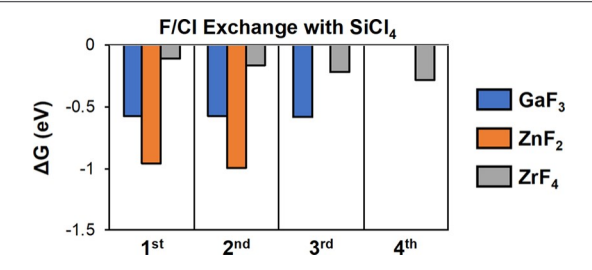


Figure 15. Thermochemical calculations for change in Gibbs free energy (ΔG) at 350 °C for sequential F/Cl exchange between SiCl $_4$ with GaF $_3$, ZnF $_2$, and ZrF $_4$.

reaction between SiCl₄ and GaF₃, ZnF₂, and ZrF₄ at 350 °C. The ligand exchange is examined for all the possible F/Cl exchanges between the SiCl₄ precursor and the metal fluoride. Figure 15 shows that GaF₃, ZnF₂, and ZrF₄ all exhibit negative ΔG values for ligand exchange with SiCl₄. These negative ΔG values support the QMS observation of metal chlorides as the metal etch products using SiCl₄ as the precursor for ligand exchange.

Figure 16 displays the ΔG values for ligand exchange between SiCl₂(CH₃)₂ and GaF₃, ZnF₂, and ZrF₄ at 350 °C. For the F/Cl exchange in Figure 16a, the ΔG values are negative for all three metal fluorides. The ΔG values are also similar to the ΔG values for SiCl₄ in Figure 15. The total F/Cl exchange

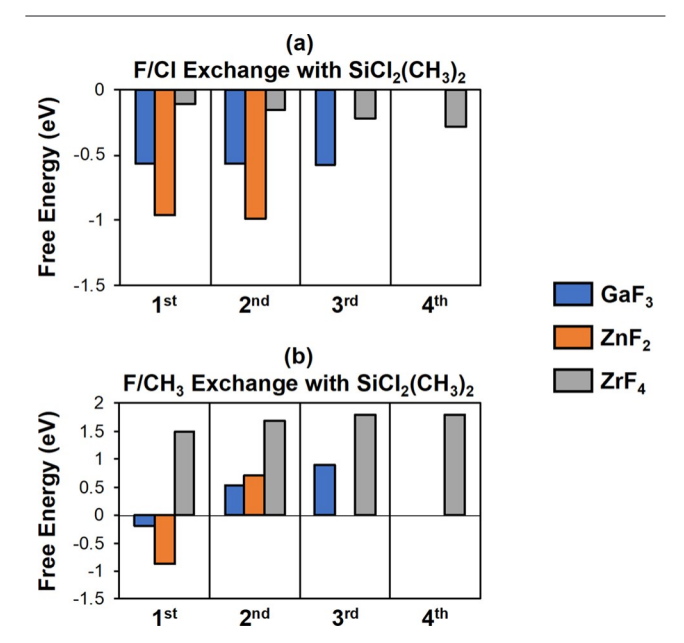


Figure 16. Thermochemical calculations of change in Gibbs free energy (ΔG) at 350 °C for sequential (a) F/Cl exchange and (b) F/CH₃ exchange between SiCl₂(CH₃)₂ with GaF₃, ZnF₂, and ZrF₄.

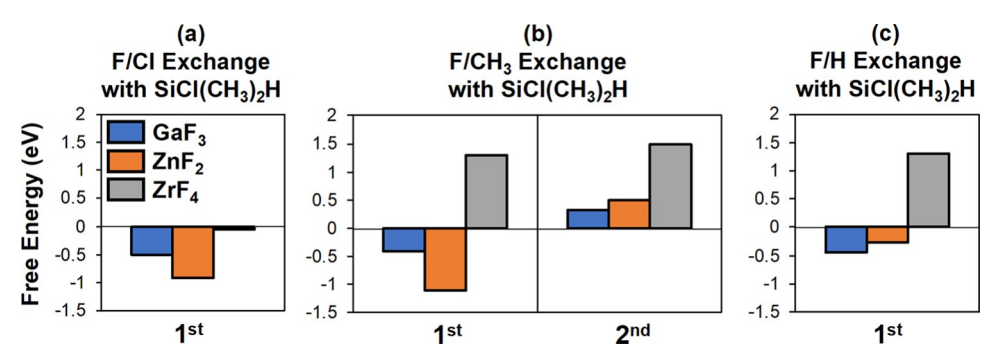


Figure 17. Thermochemical calculations of change in Gibbs free energy (ΔG) at 350 °C for sequential (a) F/CI exchange, (b) F/CH $_3$ exchange, and (c) F/H exchange between SiCI(CH $_3$) $_2$ H with GaF $_3$, ZnF $_2$, and ZrF $_4$.

between ${\rm SiCl_2(CH_3)_2}$ and the three metal fluorides is thermochemically favorable. These results support the observation of metal chlorides as metal etch products.

In contrast, Figure 16b reveals that the F/CH $_3$ exchange is only favorable for the first F/CH $_3$ exchange with GaF $_3$ and ZnF $_2$. The subsequent F/CH $_3$ exchanges have positive ΔG values for all the metal fluorides. For F/CH $_3$ exchange with ZrF $_4$, none of the F/CH $_3$ exchanges are favorable. These results agree with the lack of any observed methylated metal etch products during the QMS experiments.

Figure 17 shows the ΔG values for ligand exchange between SiCl(CH₃)₂H and GaF₃, ZnF₂, and ZrF₄ at 350 °C. Figure 17a indicates that F/Cl exchange is thermochemically favorable for all three metal fluorides. These results are consistent with the observation of metal chlorides as the metal etch products when using SiCl(CH₃)₂H as the ligand-exchange precursor. In addition, Figure 17b reveals that F/CH₃ exchange is favorable with GaF₃ and ZnF₂ only for the first F/CH₃ exchange. The second F/CH₃ exchange is thermochemically unfavorable. These results support the absence of any methylated metal etch products observed as volatile etch products during the QMS experiments.

Lastly, Figure 17c shows that F/H exchange has negative ΔG values and is favorable only between SiCl(CH₃)₂H and GaF₃ or ZnF₂. These negative ΔG values are consistent with the observation of F/H exchange for the reaction of SiCl(CH₃)₂H with GaF₃ in Figure 11b and with ZnF₂ in Figure 12b. The positive ΔG for the reaction of SiCl(CH₃)₂H with ZrF₄ in Figure 17c is also in agreement with the lack of any F/H exchange between SiCl(CH₃)₂ with ZrF₄ in Figure 13b.

The thermochemical calculations for the ligand-exchange reactions agree well with the QMS observations. The calculations determined that F/Cl exchange is favorable between all the Cl-containing silane precursors and the various metal fluorides. These results are consistent with metal chlorides as the dominant metal etch product.

4. CONCLUSIONS

The spontaneous etching of various metal fluorides with silane precursors containing different ligands was examined using *in situ* QMS investigations. The metal fluorides were GaF_3 , InF_3 , ZnF_2 , ZrF_4 , HfF_4 , and SnF_4 . The silane precursors for ligand exchange were $SiCl_4$, $SiCl_2(CH_3)_2$, $SiCl(CH_3)_2H$, and $Si-(CH_3)_4$. These homoleptic and heteroleptic silane precursors provided an evaluation of the effectiveness of F/Cl, F/CH₃, and F/H ligand exchange with the metal fluorides. Even though all the different ligands could participate in the ligand-

exchange reaction, the QMS studies revealed that F/Cl exchange was the dominant mechanism for ligand exchange. In addition, the metal chlorides $GaCl_3$, $InCl_3$, $ZnCl_2$, $ZrCl_4$, $HfCl_4$, and $SnCl_4$ were the only metal etch products resulting from the ligand-exchange reactions.

The QMS studies performed versus temperature revealed complementary behavior between the silane precursors and the silane products after the ligand-exchange reaction. During the temperature ramps, decreases/increases in the silane precursor were correlated with increases/decreases in the silane ligandexchange product. This strong correspondence argued that there was one main ligand-exchange mechanism and the dominant pathway was F/Cl exchange. Many of the correlations were also consistent with chlorine buildup that lowers the available fluorine species and reduces the ligandexchange reaction. Subsequently, metal chloride desorption exposes more fluorine species and increases the ligandexchange reaction. For a given metal fluoride, the onset temperatures for the silane ligand-exchange products were similar for all the various silane precursors. Likewise, except for SnF₄, the onset temperatures for the metal chloride etch products from a given metal fluoride were similar for all the silane precursors.

The onset temperatures for the silane ligand-exchange products were always lower than the onset temperatures for the metal chloride etch products. The differences between the onset temperatures varied between the metal fluorides. The difference was the largest for GaF₃ and InF₃, the Group 13 metal fluorides, and ZrF₄ and HfF₄, the Group 4 metal fluorides. This large difference was attributed to the dilution of CI and the slow buildup of CI in the metal fluoride before the metal chlorides can form and volatilize. In contrast, the difference was small for ZnF₂. This small difference may be related to the less favorable ligand-exchange reactions and higher onset temperatures for ligand exchange with ZnF₂.

Thermochemical calculations were also consistent with the experimental observations. ΔG calculations for F/Cl exchange yielded the most negative ΔG values compared with F/CH $_3$ or F/H exchange. These results support the observation of metal chlorides as the metal etch products. In contrast, F/CH $_3$ exchange was either not favorable or could not occur more than once with a given metal fluoride. These results support the observation that metal methyl complexes do not form as volatile metal etch products. In addition, F/H exchange is predicted for the reaction of SiCl(CH $_3$) $_2$ H with GaF $_3$ and ZnF $_2$ in agreement with the experimental observations. The experimental and theoretical results are all consistent with

dominant F/CI exchange and metal chlorides as the volatile metal etch products.



ASSOCIATED CONTENT

* Supporting Information

The Supporting Information is available free of charge at https://pubs.acs.org/doi/10.1021/acs.chemmater.2c01603.

Quadrupole mass spectrometry (QMS) results for $SiCl_4$ with $GaF_{3'}$ $ZnF_{2'}$ and ZrF_4 powder and temperature dependent QMS results for $SiCl_4$ with SnF_4 powder (PDF)

7

AUTHOR INFORMATION

Corresponding Author

Steven M. George – Department of Chemistry, University of Colorado, Boulder, Colorado 80309, United States;

orcid.org/0000-0003-0253-9184; Email: steven.george@colorado.edu

Authors

Ann Lii-Rosales – Department of Chemistry, University of Colorado, Boulder, Colorado 80309, United States

Virginia L. Johnson – Department of Chemistry, University of Colorado, Boulder, Colorado 80309, United States

Andrew S. Cavanagh – Department of Chemistry, University of Colorado, Boulder, Colorado 80309, United States;
orcid.org/0000-0002-6201-530X

Andreas Fischer – Lam Research Corporation, Fremont, California 94538, United States

Thorsten Lill – Lam Research Corporation, Fremont, California 94538, United States

Sandeep Sharma – Department of Chemistry, University of Colorado, Boulder, Colorado 80309, United States;
o orcid.org/0000-0002-6598-8887

Complete contact information is available at: https://pubs.acs.org/10.1021/acs.chemmater.2c01603

Notes

The authors declare no competing financial interest.

7

ACKNOWLEDGMENTS

This research was funded by the Lam Research Corporation. S.S. was supported through the National Science Foundation Grant CHE-2145209.

7 RI

REFERENCES

- (1) Fischer, A.; Routzahn, A.; George, S. M.; Lill, T. Thermal Atomic Layer Etching: A Review. *J. Vac. Sci. Technol. A* 2021, *39*, 030801.
- (2) George, S. M. Mechanisms of Thermal Atomic Layer Etching. *Acc. Chem. Res.* 2020, *53*, 1151–1160.
- (3) Lee, Y.; George, S. M. Atomic Layer Etching of Al_2O_3 Using Sequential, Self-Limiting Thermal Reactions with $Sn(acac)_2$ and Hydrogen Fluoride. *ACS Nano* 2015, *9*, 2061–2070.
- (4) Cano, A. M.; Marquardt, A. E.; DuMont, J. W.; George, S. M. Effect of HF Pressure on Thermal Al_2O_3 Atomic Layer Etch Rates and Al_3O_3 Fluorination. *J. Phys. Chem. C* 2019, *123*, 10346–10355.
- $(\bar{5})$ Lee, Y.; DuMont, J. W.; George, S. M. Trimethylaluminum as the Metal Precursor for the Atomic Layer Etching of Al₂O₃ Using Sequential, Self-Limiting Thermal Reactions. *Chem. Mater.* 2016, *28*, 2994–3003.
- (6) Lee, Y.; George, S. M. Thermal Atomic Layer Etching of ${\rm HfO}_2$ Using HF for Fluorination and ${\rm TiCl}_4$ for Ligand-Exchange. *J. Vac. Sci. Technol. A* 2018, *36*, 061504.

- (7) Lee, Y.; George, S. M. Thermal Atomic Layer Etching of ${\rm Al_2O_3}$, ${\rm HfO_2}$, and ${\rm ZrO_2}$ Using Sequential Hydrogen Fluoride and Dimethylaluminum Chloride Exposures. *J. Phys. Chem. C* 2019, 123, 18455–18466.
- (8) Lee, Y.; Huffman, C.; George, S. M. Selectivity in Thermal Atomic Layer Etching Using Sequential, Self-Limiting Fluorination and Ligand-Exchange Reactions. *Chem. Mater.* 2016, *28*, 7657–7665.
- (9) Zywotko, D. R.; Faguet, J.; George, S. M. Rapid Atomic Layer Etching of Al_2O_3 Using Sequential Exposures of Hydrogen Fluoride and Trimethylaluminum With No Purging. *J. Vac. Sci. Technol. A* 2018, *36*, 061508.
- (10) Murdzek, J. A.; Rajashekhar, A.; Makala, R. S.; George, S. M. Thermal Atomic Layer Etching of Amorphous and Crystalline Al₂O₃ Films. *J. Vac. Sci. Technol. A* 2021, *39*, 042602.
- (11) Murdzek, J. A.; George, S. M. Effect of Crystallinity on Thermal Atomic Layer Etching of Hafnium Oxide, Zirconium Oxide, and Hafnium Zirconium Oxide. *J. Vac. Sci. Technol. A* 2020, *38*, 022608.
- (12) Osakada, K. Transmetalation. In *Current Methods in Inorganic Chemistry*; Kurosawa, H., Yamamoto, A., Eds.; Elsevier: 2003; Vol. *3*, Chapter 5, pp 233–291.
- (13) Lee, Y.; Johnson, N. R.; George, S. M. Thermal Atomic Layer Etching of Gallium Oxide Using Sequential Exposures of HF and Various Metal Precursors. *Chem. Mater.* 2020, *32*, 5937–5948.
- (14) Johnson, N. R.; Hite, J. K.; Mastro, M. A.; Eddy, C. R.; George, S. M. Thermal Atomic Layer Etching of Crystalline GaN Using Sequential Exposures of XeF₂ and BCl₃. *Appl. Phys. Lett.* 2019, *114*, 243103.
- (15) Walsh, R. Bond-Dissociation Energy Values in Silicon-Containing Compounds and Some of Their Implications. *Acc. Chem. Res.* 1981, 14, 246–252.
- (16) Lii-Rosales, A.; Cavanagh, A. S.; Fischer, A.; Lill, T.; George, S. M. Spontaneous Etching of Metal Fluorides Using Ligand-Exchange Reactions: Landscape Revealed by Mass Spectrometry. *Chem. Mater.* 2021, *33*, 7719–7730.
- (17) Ban, V. S.; Gilbert, S. L. Chemistry and Transport Phenomena of Chemical Vapor Deposition of Silicon from $SiCl_4$. *J. Cryst. Growth* 1975, *31*, 284–289.
- (18) Bloem, J.; Claassen, W. A. P.; Valkenburg, W. Rate-Determining Reactions and Surface Species in CVD Silicon. 4. The SICl₄-H₂-N₂ and the SiHCl₃-H₂-N₂ System. *J. Cryst. Growth* 1982, *57*, 177–184.
- (19) Sone, H.; Kaneko, T.; Miyakawa, N. In Situ Measurements and Growth Kinetics of Silicon Carbide Chemical Vapor Deposition from Methyltrichlorosilane. *J. Cryst. Growth* 2000, *219*, 245–252.
- (20) Lemieux, J. M.; Zhang, J. S. Thermal Decomposition of Methyltrichlorosilane, Dimethyldichlorosilane and Methyldichlorosilane by Flash Pyrolysis Vacuum Ultraviolet Photoionization Time-of-Flight Mass Spectrometry. *Eur. J. Mass Spectrom.* 2014, *20*, 409–417.
- (21) Lee, C.; Yang, W.; Parr, R. G. Development of the Colle-Salvetti Correlation-Energy Formula into a Functional of the Electron Density. *Phys. Rev. B* 1988, *37*, 785–789.
- (22) Weigend, F.; Ahlrichs, R. Balanced Basis Sets of Split Valence, Triple Zeta Valence and Quadruple Zeta Valence Quality for H to Rn: Design and Assessment of Accuracy. *Phys. Chem. Chem. Phys.* 2005, 7, 3297–3305.
- (23) Scuseria, G. E.; Janssen, C. L.; Schaefer, H. F., III An Efficient Reformulation of the Closed-Shell Coupled Cluster Single and Double Excitation (CCSD) Equations. *J. Chem. Phys.* 1988, *89*, 7382–7387.
- (24) Scuseria, G. E.; Schaefer, H. F., III Is Coupled Cluster Singles and Doubles (CCSD) more Computationally Intensive than Quadratic Configuration Interaction (QCISD)? *J. Chem. Phys.* 1989, *90*, 3700–3703.
- (25) Dunning, T. H., Jr.; Hay, P. J. *Modern Theoretical Chemistry*; Plenum: New York, 1977.
- (26) Dill, K. A.; Bromberg, S. Molecular Driving Forces: Statistical Thermodynamics in Biology, Chemistry, Physics and Nanoscience; Garland Science: 2011.

Chemistry of Materials Article pubs.acs.org/cm

- (27) Frisch, M. J.; Trucks, G. W.; Schlegel, H. B.; Scuseria, G. E.; Robb, M. A.; Cheeseman, J. R.; Scalmani, G.; Barone, V.; Petersson, G. A.; Nakatsuji, H.; et al. Gaussian 16, Rev. C.01; Gaussian Inc.: Wallingford, CT, 2016.
- (28) Houle, F. A. Electron Impact Fragmentation of Gases by Molecular Beam Mass Spectrometery. Application to AsCl₂ and a GaCl₃/Ga₂Cl₆ Mixture. Int. J. Mass Spectrom. Ion Processes 1993, 123, 243-252.
- (29) Basner, R.; Gutkin, M.; Mahoney, J.; Tarnovsky, V.; Deutsch, H.; Becker, K. Electron-Impact Ionization of Silicon Tetrachloride (SiCl₄). J. Chem. Phys. 2005, 123, 054313.
- (30) Dibeler, V. H.; Mohler, F. L. Dissociation of SF₆, CF₄ and SiF₄ by Electron Impact. J. Res. Natl. Bur. Stand. 1948, 40, 25-29.
- (31) Brunetti, B.; Piacente, V.; Scardala, P. Vapor Pressures of Gallium Trifluoride, Trichloride, and Triiodide and Their Standard Sublimation Enthalpies. J. Chem. Eng. Data 2010, 55, 98-102.
- (32) Zywotko, D. R.; George, S. M. Thermal Atomic Layer Etching of ZnO by a "Conversion-Etch" Mechanism Using Sequential Exposures of Hydrogen Fluoride and Trimethylaluminum. Chem. Mater. 2017, 29, 1183-1191.
- (33) Matsumoto, K.; Kiba, N.; Takeuchi, T. Direct Analysis of Metal Halides by Electron Impact Mass Spectrometry. Anal. Chem. 1971, 43. 1691.
- (34) Palko, A. A.; Ryon, A. D.; Kuhn, D. W. The Vapor Pressures of Zirconium Tetrachloride and Hafnium Tetrachloride. J. Phys. Chem. 1958, *62*, 319–322.
- (35) NIST Chemistry WebBook. https://webbook.nist.gov/chemistry (accessed 2022-5-28).
- (36) Berthold, H. J.; Groh, G. Preparation of Tetramethylzirconium, Zr(CH₃)₄. Angew. Chem., Int. Ed. Engl. 1966, 5, 516-516.
- (37) Zywotko, D. R.; Zandi, O.; Faguet, J.; Abel, P. R.; George, S. M. ZrO, Monolayer as a Removable Etch Stop Layer for Thermal Al₂O₃ Atomic Layer Etching Using Hydrogen Fluoride and Trimethylaluminum. Chem. Mater. 2020, 32, 10055-10065.
- (38) Stull, D. R. Vapor Pressure of Pure Substances Organic and Inorganic Compounds. Ind. Eng. Chem. 1947, 39, 517-550.
- (39) Brunetti, B.; Piacente, V.; Scardala, P. A Torsion Study on the Sublimation Process of InCl₃. J. Chem. Eng. Data 1998, 43, 101–104.
- (40) Keneshea, F. J.; Cubicciotti, D. Vapor Pressures of Zinc Chloride and Zinc Bromide and Their Gaseous Dimerization. J. Chem. Phys. 1964, 40, 191-199.
- (41) Tangri, R. P.; Bose, D. K. Vapor-Pressure Measurement of Zirconium Chloride and Hafnium Chloride by the Transpiration Techniuque. Thermochim. Acta 1994, 244, 249-256.
- (42) Kabesh, A.; Nyholm, R. S. 716. Studies in Co-ordination Chemistry. Part X. The Vapour Pressure and Heats of Vaporisation of the Stannic Halides. J. Chem. Soc. (Resumed) 1951, 3245-3252.

□ Recommended by ACS

Solid-State Displacement Synthesis of Alkaline-Earth **Selenide for White Emission through Alternating Current** Electroluminescence

Yanze Wang, Feng Wang, et al. NOVEMBER 07, 2022 ACS MATERIALS LETTERS

READ 🗹

Electron-Enhanced Atomic Layer Deposition of Titanium Nitride Films Using an Ammonia Reactive Background Gas

Zachary C. Sobell and Steven M. George

OCTOBER 20, 2022 CHEMISTRY OF MATERIALS

READ 🗹

Sb Se Thin-Film Growth by Solution Atomic Layer **Deposition**

Vanessa M. Koch, Julien Bachmann, et al.

OCTOBER 21, 2022

CHEMISTRY OF MATERIALS

READ 🗹

Flow-Through Atmospheric Pressure-Atomic Layer **Deposition Reactor for Thin-Film Deposition in Capillary** Columns

Dhananjay I. Patel, Matthew R. Linford, et al.

MAY 17, 2022

ANALYTICAL CHEMISTRY

READ 🗹

Get More Suggestions >